Applied Ocean Research 78 (2018) 123–133

Contents lists available at ScienceDirect

Applied Ocean Research

journal homepage: www.elsevier.com/locate/apor

Dynamic model identification of unmanned surface vehicles using deep learning network

Joohyun Woo[a], Jongyoung Park[a], Chanwoo Yu[b], Nakwan Kim[c,*]

[a] Department of Naval Architecture and Ocean Engineering, Seoul National University, 1, Gwanak-ro, Gwanak-gu, Seoul, 08826, South Korea
[b] The 6th R&D institute – 3rd Directorate, Agency for Defense Development, Dong-eup, Uichang-gu, Jinhae, Changwon, 51698, South Korea
[c] Department of Naval Architecture and Ocean Engineering, Research Institute of Marine Systems Engineering, Seoul National University, 1, Gwanak-ro, Gwanak-gu, Seoul, 08826, South Korea

ARTICLE INFO

Keywords:
Unmanned surface vehicle (USV)
System identification
Deep learning
Recurrent neural network (RNN)
Long short-term memory (LSTM)

ABSTRACT

In this paper, a deep learning–based dynamic model identification method is proposed. The proposed method is designed to capture higher-order dynamic behaviors that result from the coupling of hydrodynamics and actuator dynamics. By adopting recent advancements in deep learning, our model addresses problems such as the regression problem in machine learning. Among various deep learning algorithms, long short-term memory (LSTM)–based recurrent neural network was used to deal with the hidden latent state of the USV dynamic model. The model validation was performed using free running test data of a USV. Analysis result shows that proposed model reduces surge speed prediction error by 76.9%, yaw rate prediction error by 60.7% and sway velocity prediction error by 27.9% over the conventional linear dynamic model.

1. Introduction

Over the last few decades, research on unmanned surface vehicles (USVs) has attracted considerable attention. USVs have significant advantages over conventional manned systems as they can operate in dangerous and extreme environments. Concerning commercial applications, USVs can be adopted to conduct missions such as environmental monitoring [1], resource exploration [2] or shipping [3]. For military applications, USVs are expected to perform missions such as mine countermeasures [4], anti-submarine warfare [5] and reconnaissance [6]. Although the different types of USVs have various purpose and missions, it is common that they need a robust and effective maneuvering controller for successful operation during their missions.

There have been a number of studies on the control of an USVs or ship such as [7–11]. Regarding the controller design for an unmanned system, one of the most important aspects is to understand the vehicle's dynamic behavior. Designing the controller based on its dynamics can increase both dynamic performance and stability of the vehicle. In practice, controllers of unmanned vehicles are often constructed based on identified dynamics as stated in Refs. [12,13], and [14]. To build the system's dynamic model, a method called system identification is frequently used. The system identification method finds a model that best describes input-output data relationships. In general, parameters in the system are identified through the minimization of the error between predicted output states and target output states for a given input.

Several applications of system identification methods in both time and frequency domain have been published (mostly about linear time invariant system). In the time domain approach, various system estimation methods such as maximum likelihood [15], Kalman Filter [16,17], recursive least squares [18] and particle swarm optimization (PSO) [13] have been suggested. In addition, a frequency domain approach has been suggested by Selvam et al [19].

Neural network and deep learning are also well known tools that are used for vehicle dynamic system identification. Rajesh et al [20]. proposed the black box approach, a method that uses a feed forward neural network to map the dynamical relationship between the state variable (input variable), the hydrodynamic force and moment data (output variable). Ghosh et al [21]. proposed the "delta method," which uses a feed forward neural network similar to the one adopted in Ref. [20], but in this case, the neural network is used to extract the first-order force and the moment coefficient. By making a small variation in one of the input variables, its effect on the control force or moment was calculated. Punjani et al [22]. used a rectified linear unit (RELU) based on deep neural networks, for identifying small scale helicopters. In this work, multi-layered feedforward RELU network estimated the acceleration component corresponding to the input states. Similar to aerial vehicles, there are substantial works which use neural network as a tool

* Corresponding author.
E-mail address: nwkim@snu.ac.kr (N. Kim).

https://doi.org/10.1016/j.apor.2018.06.011
Received 19 August 2017; Received in revised form 12 June 2018; Accepted 13 June 2018
Available online 23 June 2018

for modeling of a surface vehicle. This work includes [23,24] and [25]. Although such neural network–based approaches showed effective dynamics approximation capability, the methods present some limitations. Since the methods use a feed forward neural network architecture, the models cannot grasp sequential information contained in input-output history data. For example, yaw rates at time steps t and $t-1$ are strongly coupled and correlated. However, the feed forward network considers the data as independent data.

In this context, in order to grasp sequential information, a recurrent neural network (RNN)–based model was proposed for the approximation of USV dynamics. In this paper, a RNN model for predicting USV dynamics is proposed. Due to the feed-back structure of the RNN, the model has an ability to "memorize" past data pattern and able to capture the sequential information in test data. Since dynamic state at time steps t is strongly coupled to that of at time step $t-1$, such sequential information can help the model predicting its dynamics more accurately. This is one of the main contributions of this paper. Although previous works in system identification [23–25] used neural network to model dynamics, they used conventional feed-forward structure neural network. Feedback structure of RNN will increase its effectiveness by nature of ship dynamics. In addition, this paper contains a structured procedure for constructing and analyzing the dynamic modeling of a USV based on deep learning. For collecting the data set for deep learning, a free running of a USV test was conducted on a USV. For identifying the ship dynamic model, several maneuvering tests such as a turning test, zigzag test, and 3-2-1-1 input test have been performed. Using experimental data, simplified maneuvering parameters of the USV were extracted and a RNN model was used to describe the remaining terms of the USV dynamics that the simplified model cannot describe.

The remainder of this paper is organized into four main sections. In Section 2, a review of a non-linear dynamic model and a number of simplified models for USV maneuvering are presented. In Section 3, background and detailed information of RNN-based model is described. Section 4 contains the procedures for the system identification and a detailed description of the USV water test. The system identification results will be presented here, and the performance of the suggested method will be compared with the performance of other methods. In Section 5, the main conclusions and a further discussion are presented.

2. USV dynamic system

According to previous research related to USV system identification, researchers tend to choose simplified linear dynamic models such as Nomoto's model [12,13] or first-order linearized steering models [14] as a target model, because these models can be easily identified using collected free running test data. Although identified linear models are often directly used to design the controller of the USV (as in [12] and [13]), remaining non-linear parts of the dynamics of USV are important as well. In order to predict dynamic states more accurately, an additional model that considers the nonlinear parts of the dynamics has been constructed.

For this reason, the proposed dynamic model is composed of two parts. The first part is based on a simplified dynamic model of a USV. For this part, the model is identified through the same approach that Sonnenburg et al [12]. suggested. The other part of the dynamic model concerns the non-linear terms of the USV dynamic model. These terms are highly coupled and complex, due to convoluted hydrodynamics and actuator dynamics. Therefore, we decided to use a data-driven approach rather than a physics-based approach for developing this model. With high approximation and pattern extraction capability of deep neural networks, non-linear parts of the dynamic model can be extracted.

2.1. WAM-V USV

The wave adaptive modular vessel (WAM-V) is a catamaran-shaped boat platform produced by Marine Advanced Research, Inc. WAM-V platform has two inflatable pontoons, a deck, and two supporting arches [14]. One of the main characteristics of the platform is that it has two suspensions between the pontoons and vehicle's deck, which can dissipate the motion induced by waves [26,27]. The length of the WAM-V platform is 4.88 m (16 ft) and that of the beam overall is 2.44 m (8 ft). The vehicle is equipped with two electric propulsion modules (Minn Kota RT EM160) at the stern side of each hull. The maximum speed of the vehicle is approximately 4.5 knots. Because there is no rudder or gimbaled thruster (e.g., an outboard motor) as in Refs [12]. and [13], our vehicle can generate steering motion by creating RPM (revolutions per minute) differences in the two main thrusters. Because of this characteristic, there is no direct sway force acting on the vehicle, produced by the main thrusters.

Various sensors are attached to the vehicle as well. For navigation purposes, two dual frequency Novatel GPS sensors are installed to collect position, velocity and heading angle information. An AHRS sensor is mounted in the center of the deck, which provides attitude information as well as turn rate information. National Instrument cRIO-9024 model is used to collect navigational sensor data and to calculate the control command of the USV. In addition, sensor data and control input histories are logged in the computer during maneuvering tests.

2.2. USV dynamic model

In order to depict the motion of the WAM-V USV, we have derived an equation of motion for rigid hull with a differential thruster. For simplicity, we consider only three degrees of freedom (surge, sway and yaw) in the horizontal planar motion. The notation developed by Fossen was adopted [28,29]. Fig.1 shows a schematic description of the USV and its coordinate frame, where x_i and y_i represent, respectively, the north and east directions of the vehicle in the inertial frame while u, v and V represent the surge, sway and total speed of the vehicle in a body fixed frame, respectively. The heading angle of the vehicle is represented as ψ, while the side slip angle and the course angle are defined by χ and β, respectively. The side slip angle can be calculated by the expression $\beta = \arcsin(\frac{v}{V})$ and the course angle can be defined using the heading angle and the side slip angle as $\chi = \psi + \beta$.

The kinematic model of the USV can be expressed by the following equation.

$$\dot{\boldsymbol{\eta}} = \boldsymbol{R}(\boldsymbol{\eta})\boldsymbol{\nu} \tag{1}$$

where $\boldsymbol{\nu}$ is the velocity vector, $\boldsymbol{\eta}$ is the position vector and $\boldsymbol{R}(\boldsymbol{\eta})$ is a rotation matrix that maps vectors from a body fixed frame to an inertial frame.

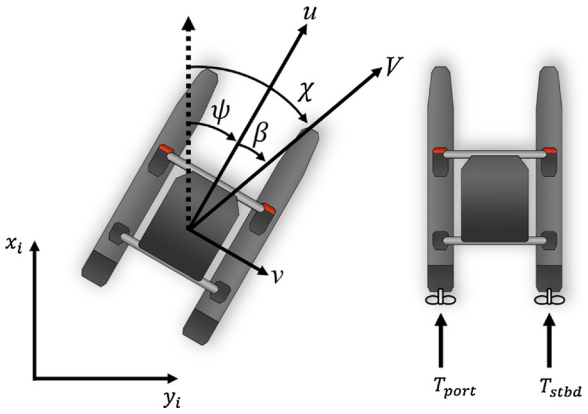

Fig. 1. Schematic description of the diffrential thrust of the USV.

$$\boldsymbol{\nu} = (u\ v\ r)^T \tag{2}$$

$$\boldsymbol{\eta} = (x_i\ y_i\ \psi)^T \tag{3}$$

$$\boldsymbol{R}(\boldsymbol{\eta}) = \begin{bmatrix} \cos\psi & -\sin\psi & 0 \\ \sin\psi & \cos\psi & 0 \\ 0 & 0 & 1 \end{bmatrix} \tag{4}$$

The planar dynamics of the surface vehicle can be expressed by the following equation.

$$\boldsymbol{M}\dot{\boldsymbol{\nu}} + \boldsymbol{C}(\boldsymbol{\nu})\boldsymbol{\nu} + \boldsymbol{D}(\boldsymbol{\nu})\boldsymbol{\nu} = \boldsymbol{f} \tag{5}$$

where $\boldsymbol{M}$ is the mass matrix, which is composed of rigid body mass and added mass, $\boldsymbol{C}$ is the Coriolis and centripetal matrix, $\boldsymbol{D}$ is **the** damping matrix, which contains damping parameters, and $\boldsymbol{f}$ represents the control forces and moment. For details of the dynamic model, we adopted a physics-based nonlinear dynamic model suggested in Ref. [12]. Since the propulsion system of the WAM-V USV is a differential thruster type, $\boldsymbol{f}$ can be described as a function of T_{port} and T_{stbd} according to the following equation.

$$\boldsymbol{f} = \begin{bmatrix} \tau_X \\ \tau_Y \\ \tau_N \end{bmatrix} = \begin{bmatrix} T_{port} + T_{stbd} \\ 0 \\ (T_{port} - T_{stbd})B/2 \end{bmatrix} \tag{6}$$

where T_{port} and T_{stbd} are the thrust force of the port side thruster and the starboard side thruster, respectively, and B refers to the beam of the WAM-V USV.

Combining all, the three degree of freedom nonlinear dynamic model of the USV can be described by the following equations.

$$(m - X_{\dot{u}})\dot{u} - m(x_G r^2 + vr) + Y_{\dot{v}} vr + \frac{Y_{\dot{r}} + N_{\dot{v}}}{2} r^2 + X_u u + X_{|u|u}\ |u|\ u = \tau_X \tag{7}$$

$$(m - Y_{\dot{v}})\dot{v} + (mx_G - Y_{\dot{r}})\dot{r} + (m - X_{\dot{u}})ur + Y_v v + Y_r r + Y_{|v|v}\ |v|\ v + Y_{|r|r}\ |r|\ r = \tau_Y \tag{8}$$

$$(mx_G - N_{\dot{v}})\dot{v} - (I_{zz} - N_{\dot{r}})\dot{r} + mx_G ur - Y_{\dot{v}} uv - \frac{Y_{\dot{r}} + N_{\dot{v}}}{2} ur + X_{\dot{u}} uv + N_v v + N_r r + N_{|v|v} \left|v\right| v + N_{|r|r} \left|r\right| r = \tau_N \tag{9}$$

where $X_{(\cdot)}$, $Y_{(\cdot)}$ and $N_{(\cdot)}$ represent constant hydrodynamic coefficients, which are partial derivatives of surge, sway force and yaw moment, respectively, with respect to the subscript variable.

Since the USV is operated in relatively confined environment where environmental disturbance can be neglected, we may neglect any coupling between horizontal plane motions (surge, sway and yaw) [12]. Therefore, USV equation of motion can be simplified into the followings speed and steering dynamics equations.

2.2.1. Speed dynamics

In order to obtain a simplified speed dynamic equation, we linearize Eq. (7) according to the linearization point below:

$$u = u_0\ m/s,\ v = 0\ m/s,\ r = 0\ deg/s,\ \tau_X = \tau_{X0}\ N,\ \tau_N = 0\ N{\bullet}m \tag{10}$$

Next, the perturbation dynamics can be simplified as a first-order linear dynamics.

$$\Delta\dot{u} = a_u \Delta u + b_u \Delta\tau_X \tag{11}$$

where Δu and $\Delta\tau_X$ refers to the perturbation of surge speed and thrust, which are defined as $\Delta u = u - u_0$ and $\Delta\tau_X = \tau_X - \tau_{X0}$. Eq. (11) can be written in terms of non-perturbation variables resulting in the simplified speed dynamic equation near the linearization point as follows.

$$\dot{u} = a_u u + b_u \tau_X + b_{u_{bias}} \tag{12}$$

2.2.2. Steering dynamics

For the steering dynamics (sway and yaw motion), following three simplified models are frequently used.

Nomoto's steering model is suggested by Nomoto et al. [30] and describes the relationship between the yaw rate (r) and the rudder angle (δ). Since WAM-V USV is a differential thruster type, control moment (yaw direction) (τ_N) is used as a control input instead of rudder angle (δ) as shown below.

$$\tau\dot{r} + r = K_r \tau_N + b_{r_{bias}} \tag{13}$$

Nomoto's steering model with sideslip is a model suggested by Yu et al. [31], which extends the concept of Nomoto's steering model toward sideslip. A first-order lag model was suggested in order to consider the sideslip as stated in Eq. (14).

$$\tau_\beta\dot{\beta} + \beta = -K_\beta r + b_{\beta_{bias}} \tag{14}$$

Combining Eq. (13) and Eq. (14), Nomoto's steering model with sideslip can be described as follows.

$$\begin{pmatrix} \dot{\beta} \\ \dot{r} \end{pmatrix} = \begin{pmatrix} -\frac{1}{\tau_\beta} & -\frac{K_\beta}{\tau_\beta} \\ 0 & -\frac{1}{\tau_r} \end{pmatrix} \begin{pmatrix} \beta \\ r \end{pmatrix} + \begin{pmatrix} 0 \\ \frac{K_r}{\tau_r} \end{pmatrix} \tau_N + \begin{pmatrix} b_{\beta_{bias}} \\ b_{r_{bias}} \end{pmatrix} \tag{15}$$

Linear steering dynamic model is a physics-based model, which can be obtained by linearizing the non-linear steering model presented by Eqs. (8) and (9), at the linearization point stated by Eq. (10). As in Nomoto's steering model with sideslip, linear steering dynamic model can also consider sway motion. Nomoto's steering model with sideslip shows that the sideslip angle was only induced by the yaw rate. However, in the linear steering dynamic model, sway velocity is affected by not only the yaw rate, but also by the rudder input (in our case, direct control moment).

$$\begin{pmatrix} \dot{v} \\ \dot{r} \end{pmatrix} = \boldsymbol{A} \begin{pmatrix} v \\ r \end{pmatrix} + \boldsymbol{B}\tau_N + \boldsymbol{B_{bias}} \tag{16}$$

where $\boldsymbol{A}$ matrix refers to a 2 by 2 system matrix, $\boldsymbol{B}$ and $\boldsymbol{B_{bias}}$ are 2 by 1 vectors.

Among the three simplified steering models, we have chosen linearized steering dynamic model as our base model, which will be compared with our LSTM model for steering dynamic prediction. In the next section, we will explain the architecture of the deep learning method that was used and its application to a USV dynamic model representation.

3. LSTM-based dynamic model

3.1. Long short-term memory (LSTM)

LSTM is one kind of recurrent neural network. RNN is known as a branch of deep learning, that takes the advantage of its feed-back loop structure to store and memorize past information, reducing the complexity and number of layers in its structure [32]. Because of the feedback loop structure and its ability to learn the temporal feature of the data, RNN is widely used to learn time-series data.

LSTM structure is proposed by Hochreiter et al [33]. in attempt to solve vanishing gradient and divergence problems that occurs in conventional RNN structures. LSTM structure is composed of a cell with a number of gates attached. By opening and closing the gates, LSTM can truncate gradients in the network. The following equations show the mathematical formulation of LSTM [34,35].

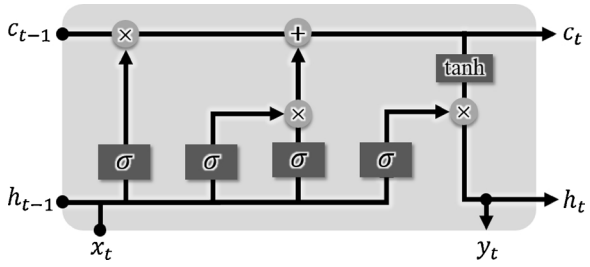

Fig. 2. Schematic architecture of the LSTM method.

$$
\begin{aligned}
i_t &= \sigma(W_{xi}x_t + W_{hi}h_{t-1} + b_{ii}) && \text{Input gate}\\
f_t &= \sigma(W_{xf}x_t + W_{hf}h_{t-1} + b_{if}) && \text{Forget gate}\\
z_t &= \tanh(W_{xc}x_t + b_c) && \text{Block input}\\
c_t &= f_t \odot c_{t-1} + i_t \odot z_t && \text{Cell state}\\
o_t &= \sigma(W_{xo}x_t + W_{ho}h_{t-1} + b_{io}) && \text{Output gate}\\
h_t &= o_t \odot \tanh(c_t) && \text{Block output}
\end{aligned} \tag{17}
$$

where x_t is the input vector at a time step t, $W_{(\cdot)}$ and $b_{(\cdot)}$ represent the weight matrix and the bias vector for linear transformation, $\sigma(\bullet)$ refers to the element-wise activation function (normally sigmoid function) and $\odot$ denotes the point-wise vector products. Note that the network can control the information flow by opening and closing the input, output and forget gates. Fig. 2 depicts the schematic architecture of LSTM.

3.2. LSTM for dynamic model identification

Considering a USV dynamical system with state vector x and input u, the non-linear dynamic equations given by Eq. (7) to (9) can be generalized into the following form.

$$\dot{x} = F(x, u) \tag{18}$$

By using the linear time-invariant representation of the system equation, Eq. (18) can be expressed as follows.

$$\dot{x} = F_{Linear}(x, u) + F_{H.O.T}(x, u) \tag{19}$$

In the above equation, the system equation is composed of linear terms (F_{Linear}) and non-linear (higher-order term) parts ($F_{H.O.T}$). The goal of the LSTM architecture is to capture the dynamic behavior of the non-linear higher-order term with respect to the current state and input. By differentiating experiment data, state rate $\dot{x}$ data can be collected, and F_{Linear} can be calculated by the identified simplified dynamic model. Afterward, the target data of non-linear parts of the dynamics can be calculated. Once the desired non-linear state rate is calculated, LSTM will learn the dynamic pattern of $F_{H.O.T}$ with respect to the input variables throughout the training process. The network was trained using the Adam optimization method [36]. The goal of the optimization process is to minimize the following loss function.

$$\mathscr{L} = \sum_{t=1}^{T} \frac{1}{T} \| \widetilde{F}_t - F_{Linear}(x_t, u_t) - F_{H.O.T}(x_t, u_t, \theta) \|^2 \tag{20}$$

where t and T are the time step and the length of the training data, $\widetilde{F}_t$ is the observed value of state rate in experiment data at time step t, and θ is the set of weight and bias parameters in the LSTM-based dynamic model. Fig.3 shows LSTM architecture and the schematic description of its application to a dynamic system identification problem. In this study, independent models for each degree of freedom are constructed for dynamics approximation.

4. System identification

In order to identify the dynamic model of the USV, a number of experiments have been performed. The experiments include turning test, zigzag test and 3-2-1-1 input test. The experiment was performed in the Lake PyoungTaek (Korea) in mild weather conditions. Thus, we assumed that the effect of environmental disturbance can be neglected. This can be seen as too ideal assumption, however, since our prime purpose is identifying dynamics of the vehicle, it is reasonable to isolate it from the effect of external disturbance. Such effect can be considered in the later stage (e.g. for maneuvering simulation) by adding environmental disturbance model.

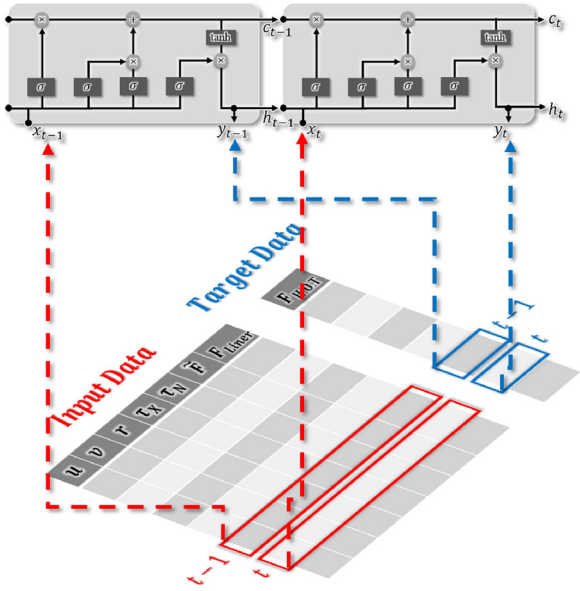

Fig. 3. Schematics description of LSTM model used for dynamic system identification.

This section is composed of four parts. Firstly, an actuator dynamics identification is suggested in sub-Section 4.1. Next, the identification process of a simplified maneuvering model is explained in sub-Section 4.2. Knowing the linear dynamic model, an LSTM-based dynamic model that describes non-linear dynamics is proposed in 4.3. Finally, the identification results are presented in Section 4.4.

4.1. Actuator dynamics

The WAM-V platform is equipped with two independent electric thruster modules as illustrated in Fig. 1. Since our proposed dynamic model directly uses the control force and the moment as input variables for the system, the dynamical behavior of the actuator must be determined in advance for ship dynamics identification. In order to do that, we have performed three different actuator–related tests.

Firstly, the relationship between the electric motor throttle and the steady state RPM must be identified. Since there is no encoder installed in the thruster module itself, we needed to measure motor revolution directly from the propeller axis. This can be done by connecting the propeller axis to a 360-° turntable potentiometer through a flexible coupling. Measuring the voltage signal while the propeller is rotating will generate a periodic voltage output. By calculating the time period between the periodic signals, the elapsed time for a revolution can be determined. Fig.4 describes the relationship between the motor throttle and RPM. We found that the relation can be expressed as a linear function, having absolute value bound at approximately 2380 RPM.

After the steady state relationship between motor throttle and RPM is identified, it is necessary to describe the transient behavior of the motor as well. In order to do so, a simplified RPM model was adopted as shown in Fig.5.

By adopting a saturation rate for the propeller speed δn (in RPM), the RPM rate $\dot{\delta n}$ is limited by a maximum value $\dot{\delta n}_{max}$. This part of the RPM model can express a time delay between the RPM command δn_{cmd}

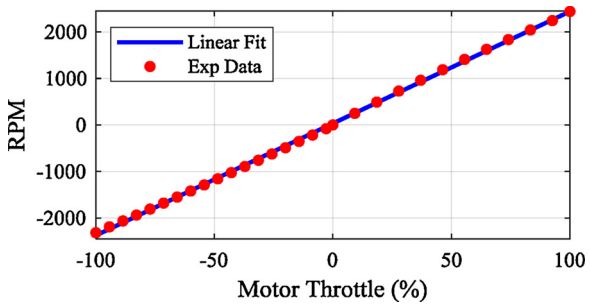

Fig. 4. Relationship between electric motor throttle and steady state RPM.

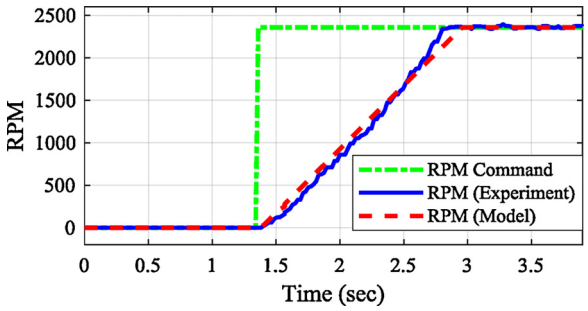

Fig. 6. Step response test result of an electric thruster motor.

and the actual RPM δn. Using the relationship between the motor throttle and the steady state RPM suggested in Fig.4, δn_{max} is determined as 2,380. However, $\dot{\delta n}_{max}$ still needs to be identified. In order to find this parameter, we performed step response tests in the electric motor. Fig.6 shows the result of one of the step response tests of the thruster motor. At 1.35 s, the RPM command (green dash-dot line) value is stepped up as maximum RPM. Collected data of RPM during the experiment is shown by the blue line. In order to consider the time delay effect, we have set $\dot{\delta n}_{max}$ value as 1,500. As a result, the simplified RPM model can approximate the dynamic behavior of RPM, what can be shown by the red dashed line, which presents a similar transient behavior.

As mentioned above, the system input in our dynamic system model equation is defined as the control force and the moment component generated by thrusters. Therefore, it is essential to find out the amount of force that the electric motors can generate. To find out the relationship between the motor's RPM and the thrust force, a bollard-pull test was conducted. In the bollard-pull test, WAM-V is tethered to a pier (fixed point) and a tension scale is attached to the tether in order to measure thrust force. Fig. 7(a) is a snapshot of bollard-pull test environment and Fig.7(b) shows the test result in various RPM conditions. The test results indicate the total net force acting on the tether, being thrust forces generated by both starboard and port side motors included. For the forward revolution of the motor, the maximum thrust force measured is 846.1 N and a quadratic model can be extracted as shown by the green line in Fig.7(b). A bollard-pull test with reverse revolution of the motor is also conducted. The maximum backward thrust measured was 429.8 N and the quadratic model of the backward thrust force with respect to RPM is given by the red line in Fig.7(b).

Using the result of the bollard-pull test, the thrust force of the electric motor (either starboard or port side) can be estimated by the following equations.

Forward RPM revolution

$$T = 3.54 \times 10^{-5}\delta n^2 + 0.084\delta n - 3.798 \quad (21)$$

Reverse RPM revolution

$$T = -1.189 \times 10^{-5}\delta n^2 + 0.0707\delta n + 4.331 \quad (22)$$

However, during the test, WAM-V is tethered to the pier and the surge speed effect on the thrust force (due to the propeller's advanced speed) cannot be considered in this model.

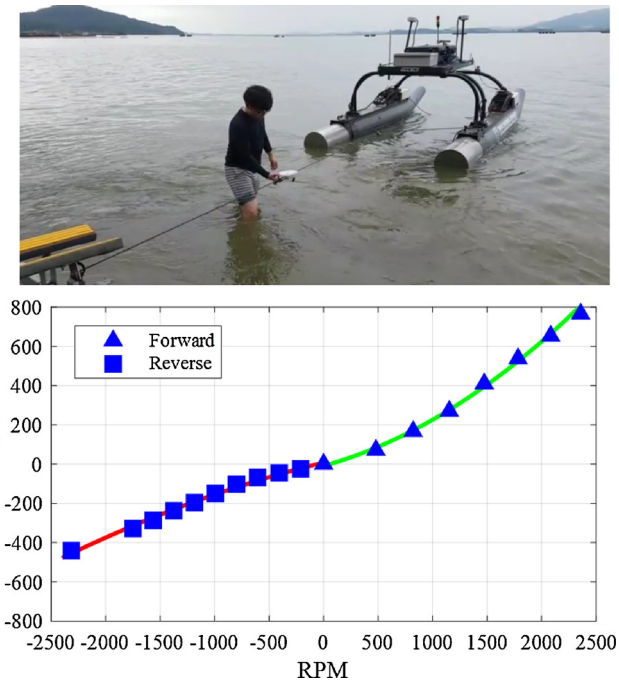

Fig. 7. Experiment result of a Bollard-pull test: (a) Bollard-pull test environment and (b) Relationship between motor RPM and thrust force.

4.2. Simplified maneuvering model

To describe the ship dynamic behavior, both speed and steering dynamics have to be identified. The simplified models covered by Eqs. (12) and (16) will be used as target models for the identification. Once the models are identified, the simplified model will be compared with the LSTM-based dynamic model, for validation of its dynamic prediction capability.

4.2.1. System identification strategy

For the identification of the simplified maneuvering model, the system identification method suggested in Ref [12]. will be used to extract the model parameters. In this method, a number of steady state constraint equations are constructed based on constant input tests. To determine dynamic parameters, test data of the dynamic input test is used. Detailed explanation about the system identification method is

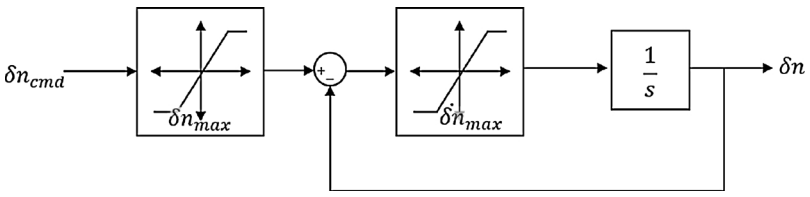

Fig. 5. Simplified block diagram of the RPM model.

listed below.

Consider a linear and time invariant system with a bias term.

$$\dot{x} = Ax + Bu + B_{bias} \tag{23}$$

where $x(t) \in \mathbb{R}^n$, $u(t) \in \mathbb{R}^m$ and A, B and B_{bias} matrix are real matrices. System identification in this case refers to extracting $n(n + m + 1)$ parameters in the system model. By assuming that A is Hurwitz and constant input u_{ss} is applied to the system, the state will eventually reach a steady state. By collecting sufficiently large set of steady state input data, the following constraints can be derived.

$$x_{ss} = \Phi u_{ss} + \Phi_{bias} \tag{24}$$

where Φ and Φ_{bias} are steady state–input constraint matrix $(n \times m)$ and vector $(n \times 1)$, respectively. Parameters in the constraints can be derived by least square estimation of the dataset matrix equation. Substituting Eq. (24) into Eq. (23) during steady state gives,

$$0 = Ax_{ss} + Bu_{ss} + B_{bias} = (A\Phi + B)u_{ss} + (A\Phi_{bias} + B_{bias}) \tag{25}$$

Then, the following constraint equation can be derived as follows.

$$0 = A\Phi + B \tag{26}$$

$$0 = A\Phi_{bias} + B_{bias} \tag{27}$$

Eqs. (26) and (27) constrain the choice of selecting remaining model parameters. Once such constraints are extracted, the remaining model parameters are extracted from dynamic input tests such as zigzag and 3-2-1-1 input tests.

Experiment data contains time history of states $x(t)$ and control input $u(t)$. In addition, by applying signal filter and taking derivatives of state variables, the state rate $\dot{x}(t)$ can be calculated. According to Eqs. (26) and (27), matrix B and B_{bias} can be written as:

$$B = -A\Phi \text{ and } B_{bias} = -A\Phi_{bias} \tag{28}$$

Substituting Eq. (28) into Eq. (23) gives,

$$\dot{x}(t) = A(x(t) - \Phi u(t) - \Phi_{bias}) \tag{29}$$

With the experiment data, every variable listed in Eq. (29), except for the system matrix A, is already known (measured). Thus, by using least square estimation method, parameters in A matrix can be derived. Once the system matrix A is identified, B and B_{bias} can be derived using the steady state constraints (Eq. (28)).

4.2.2. Maneuvering test

To achieve the steady state relationship between the state and the control input, a constant input test of the USV has been performed. For simplicity of the input variable condition, we have defined the control command variables δ_{nm} and δ_{nd}. Both variables are normalized variables, having a constant value between -1 and 1. δ_{nm} refers to the normalized mean value of the starboard and port side thruster RPM. On the other hand, δ_{nm} is defined as a normalized RPM difference of the two thrusters.

$$\delta_{nm} = (\delta_{n\,port} + \delta_{n\,stbd})/2\delta_{n\,max} \tag{30}$$

$$\delta_{nd} = (\delta_{n\,port} - \delta_{n\,stbd})/2\delta_{n\,max} \tag{31}$$

Fig.8 describes some of the test results of the constant input test (turning test). Fig.8(a) shows a video snapshot during the turning test experiment and Fig.8(b) depicts the trajectory of the WAM-V during the turning test with various control command inputs. Since the WAM-V has differential thruster, as δ_{nd} decreases, the diameter of the turning trajectory tends to increase. In addition, the turning case $\delta_{nm} = 0$ and $\delta_{nd} = 1.0$ (blue solid line) implies full forward thrust on port thruster and full reverse thrust on starboard side. Since there is distinctive difference in maximum thrust force magnitude in forward and reverse thrust, the vehicle tends to make turning motion, rather than pivoting (pure yaw motion without making surge and sway motion).

We have conducted 60 constant input tests, and by collecting steady

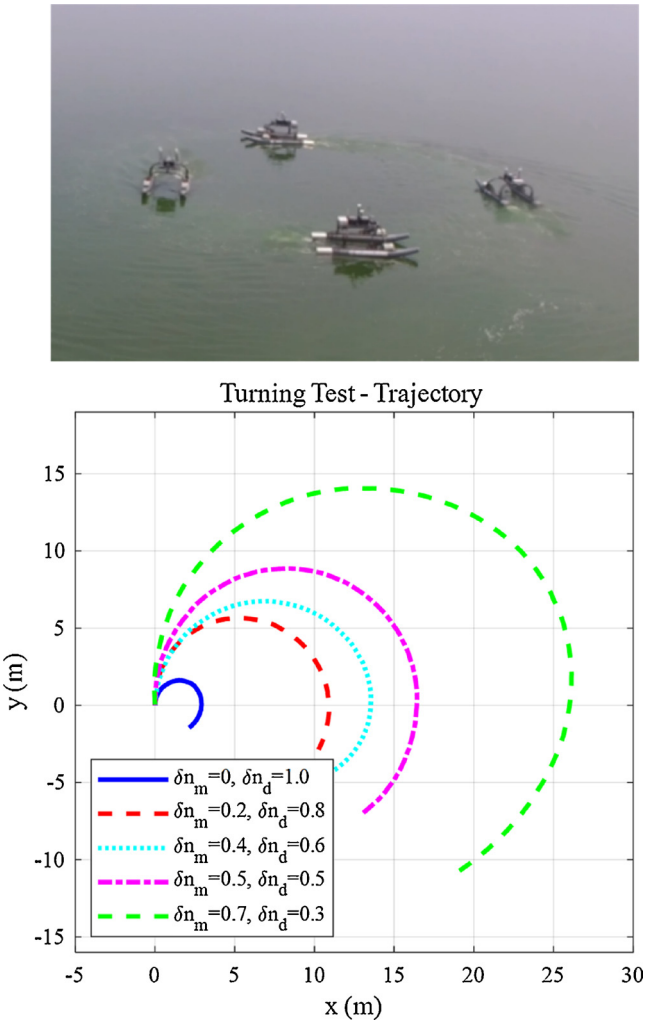

Fig. 8. Test result of the constant input test (a) Video snapshot of WAM-V conducting turning test and (b)Trajectory of WAM-V during turning tests with various input commands.

state results, a look up table that relates constant input and steady state variables can be built. Fig. 9 shows a visual relationship between the constant input and steady state variables. Since the constraint extracted from the relationship should be directly applicable to the system model, we have transformed the test commands δ_{nm} and δ_{nd} into the corresponding control force (τ_X) and moment (τ_N), variables that use the identified actuator dynamics.

Having the steady state look up table, the constraints mentioned in section 4.2.1 can be calculated. For the identification of both speed dynamics and steering dynamics, the constraint equations required for the simplified model identification are listed below.

$$\begin{aligned} u_{ss} &= \Phi_u \tau_{X_{ss}} + \Phi_{u_{bias}} \\ v_{ss} &= \Phi_v \tau_{N_{ss}} + \Phi_{v_{bias}} \\ r_{ss} &= \Phi_r \tau_{N_{ss}} + \Phi_{r_{bias}} \end{aligned} \tag{32}$$

where $\Phi_{(\cdot)}$ refers to parameters for the constraint equation. Using the least square method, parameter values are derived and their values are expressed in Table 1.

Remaining parameters of the system's model will be extracted from dynamic input test results. For the speed dynamics, acceleration-deceleration tests have been conducted. During the test, δ_{nd} is fixed to 0, for isolating speed dynamic from steering dynamics. δ_{nm} command is stepped up and down repeatedly so that it can stimulates the transient behavior of the speed dynamics. Fig. 10 depicts the results of the

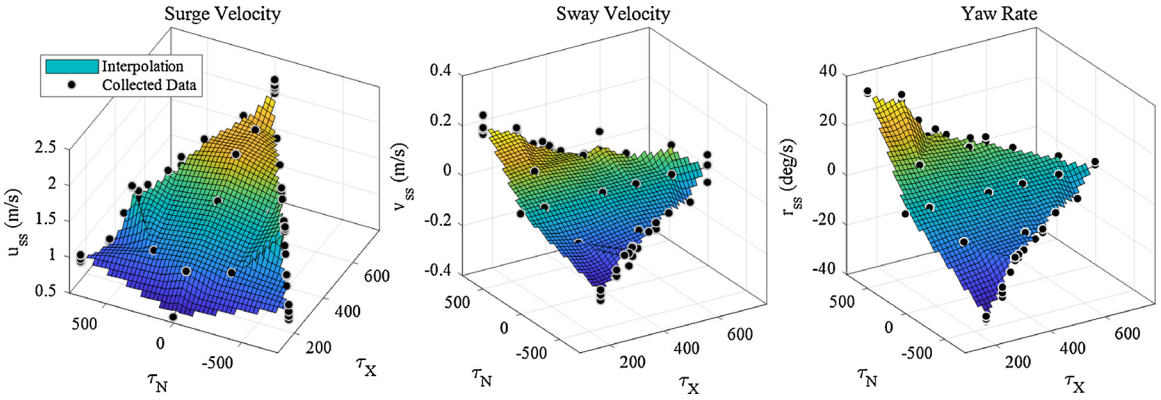

Fig. 9. Steady state result of the constant input test with respect to various control input conditions.

Table 1
Steady state constraint parameter values.

Model	Parameters
Speed Dynamics	Φ_u: 0.0021 Φ_{ubias}: 0.5182
Linear Dynamics	Φ_v: 2.23×10^{-4} Φ_{vbias}: − 0.007
	Φ_r: 0.341 Φ_{rbias}: 0.657

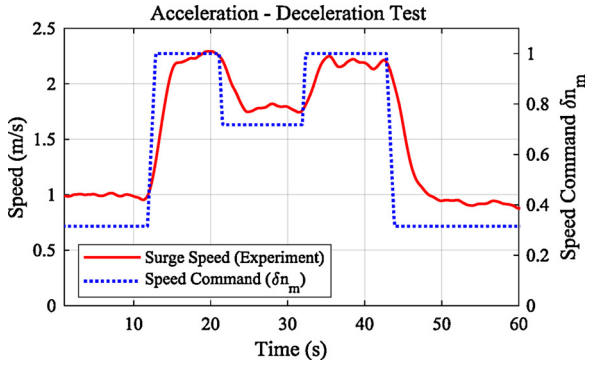

Fig. 10. Result of an acceleration-deceleration test for speed dynamics identification.

acceleration-deceleration test. For the steering dynamics, zigzag tests with a number of command conditions have been conducted. Zigzag tests are maneuvers that repeatedly switch vehicle's steering control command sign, when its heading angle reaches predefined bounds. Fig. 11(a) shows a video snapshot of the zigzag test of the WAM-V, and Fig. 11(b) represents heading angle and control commands δ_{nd} during the test. The test condition of the zigzag test in Fig. 11(b) is 10°/0.5 (heading bound and control command respectively), which results in a control input sign change when it reaches the heading angle bound (±10 °). Fig.11(c) shows the trajectory of WAM-V during the zigzag test with various test command conditions. In addition to the zigzag test, a number of 3-2-1-1 tests are also performed to capture the transient dynamic behavior of USV. The 3-2-1-1 tests are maneuvers that are composed of positive and negative step input with contiguous time steps, proportional to 3, 2, 1 and 1 period. The 3-2-1-1 test is designed by *Marchand and Koehler* [37] for identification of aircraft parameter estimation. It is widely used method since it can excite the broad range of frequency spectrum of the system's dynamic response. Fig.12 shows an example of the conducted 3-2-1-1 test result. In Fig.12, the steering command δ_{nd} is proportional to 3, 2, 1 and 1 period. In this case, the period is set as 3 sec and the amplitude of the input command is set as 1. With varying period and amplitude, total 10 3-2-1-1 test have conducted.

Although state variables of the model can be directly measured from

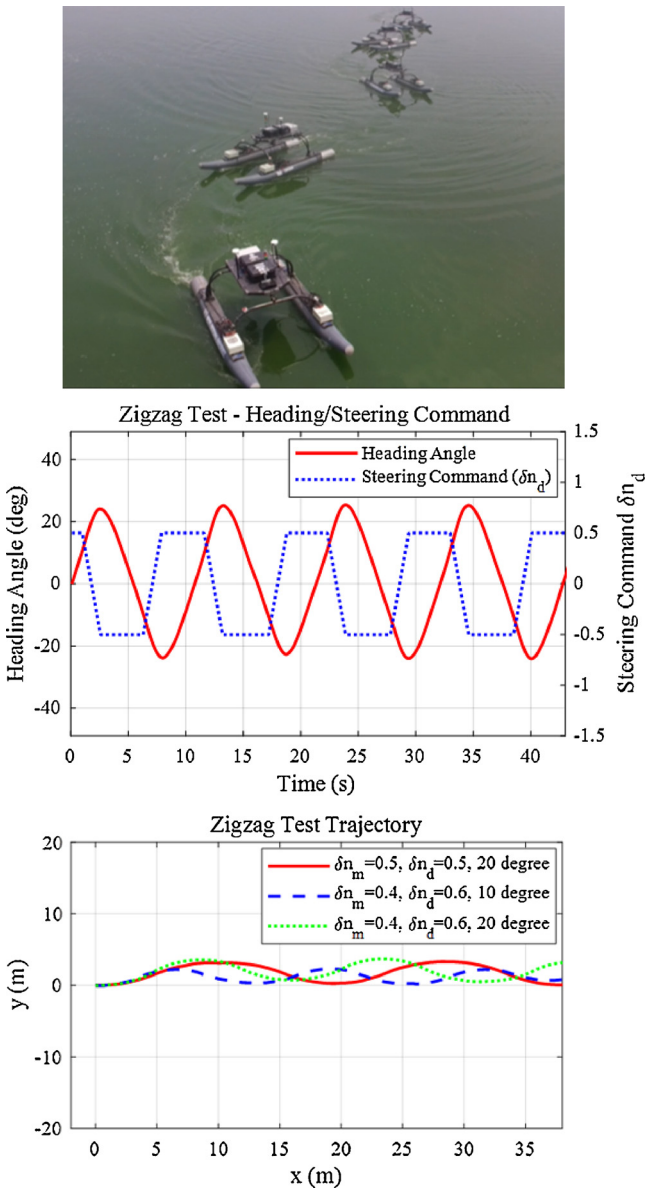

Fig. 11. Result of zigzag test for steering dynamics identification. (a) Video snapshot of WAM-V during a zigzag test. (b) Heading angle and steering command during a 10°/0.5 zigzag test (c) Trajectory of WAM-V during zigzag tests with various test conditions.

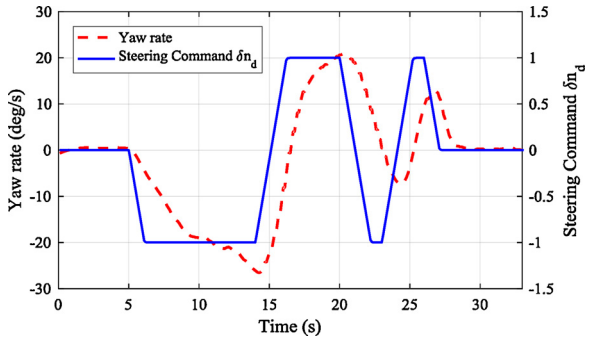

Fig. 12. Result of 3-2-1-1 test for steering dynamics identification.

navigational sensors, state rate information should be calculated by differentiating the collected state data. During that process, noise in measurement data tends to be magnified, resulting in a poor signal condition. To avoid this tendency, we have applied Savitsky-Golay filter [38] to the measurement data. This filter generates a polynomial fitting curve based on the data points in a moving window. Derivatives of the data points can be calculated by differentiating the polynomial curves.

Throughout this study, a total of 126 maneuvering tests have been conducted for the identification purpose. This includes 60 sets of static input tests, 50 zigzag tests, 6 acceleration–deceleration tests and 10 3-2-1-1 input tests. Among the test data set, a static input test, such as a turning test, is used for calculating steady state input-output constraints (Eq. (32)). The rest of the experiment data is then divided into two data sets, which are training set and validation set. The reason why we have divided data set is to accurately evaluate the constructed model with unseen data. For this, we have randomly selected 46 test data out of 66 test, (4 from acceleration–deceleration test, 36 from zigzag test, 6 from 3-2-1-1 test data) and used the data sets for extracting model parameters (training set). The remaining 20 test data sets (validation set) are never used in the model identification process, thus it is suitable for evaluating the model's prediction capability. If a performance of the constructed model with validation set data is comparable to that of with training set, we may say that the model possesses enough ability to predict the vehicle's dynamics.

Based on the training data set and method suggested in Section 4.2.1, simplified maneuvering model parameters are identified by Eqs. (33) to (34). The unit of the sideslip angle and the yaw rate are degrees and degrees per second, respectively.

Linear speed dynamic model

$$\dot{u} = -1.3191u + 0.0028\tau_X + 0.6836 \tag{33}$$

Linear steering dynamic model

$$\begin{pmatrix}\dot{v}\\ \dot{r}\end{pmatrix} = \begin{pmatrix}0.0161 & -0.0052\\ 8.2861 & -0.9860\end{pmatrix}\begin{pmatrix}v\\ r\end{pmatrix} + \begin{pmatrix}0.0002\\ 0.0307\end{pmatrix}\tau_N + \begin{pmatrix}0.0068\\ 1.3276\end{pmatrix} \tag{34}$$

Fig.13 shows a comparison result between the simplified steering models. To compare each model's performance, we have conducted identical zigzag test simulations based on each identified model. During the simulation, the same control input history that was used in experimental the zigzag tests was applied to each model. In Fig. 13, the red line refers to experimental data of sway velocity and yaw rate, while other colored line contains the simulation result of the corresponding models. Since the Nomoto's steering model does not have ability to depict sway velocity, its value is set as 0. As a result of the comparison, linear steering model (blue dash-dot line) tends to have the least error among the three simplified steering models.

4.3. LSTM-based dynamic model

Although simplified maneuvering model can approximate the dynamic behavior of the USV as in Fig. 13, due to the limitation of the

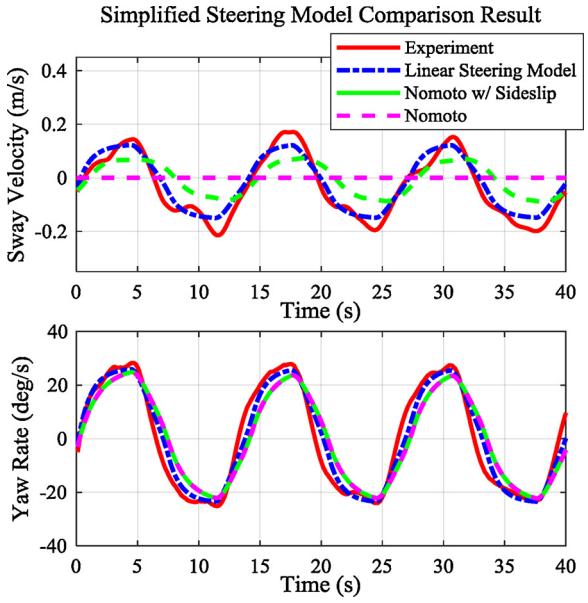

Fig. 13. Simulation results of a zigzag test using extracted simplified steering models.

model structure, it cannot fully capture complex non-linear effects in USV dynamics. To overcome this limitation, we have adopted LSTM architecture to estimate the non-linear effect of the dynamics. For training the LSTM network, the same training data set used to identify the linear steering model is used. The training data set for steering dynamics is composed of 36 zigzag test data set and six 3-2-1-1 input test data set. The data contains the time history of position, velocity, orientation, angular rate, and control input of USV with sampling rate of 20 Hz. For the neural network structure, basic LSTM cell structure with 100 hidden nodes is used. To prevent overfitting to the training data, Dropout technique [39] is adopted. For the activation function, soft sign function is used. Three independent LSTM models are constructed to deal with each degree of freedom (surge, sway, and yaw). Each model possesses 42,101 weights and bias variables which should be trained. For the training process of the LSTM, along with state and input variables of the system equation, state rate information predicted from linear steering dynamic model is necessary (see Section 3.2 for details). An Adam optimizer was used for training the network, with the learning rate set at 1×10^5 for 200,000 iterations.

Figs. 14 and 15 show the performance of the LSTM model for estimating speed dynamics and steering dynamics of the USV, compared to conventional simplified dynamic model. In the figures, the red solid line shows the experiment data measured from the navigational sensors. To compare each model, one of the validation data set is selected for both speed dynamics and steering dynamics. For the speed model comparison result, an acceleration-deceleration test result in validation data set is used, while a zigzag and 3-2-1-1 test result in the validation data set is used for the steering model comparison result. By running forward simulation with each dynamic models, we can compare each model's dynamics prediction capability. Green dashed line and blue dash-dot lines refer to the state prediction result using linear dynamic model and LSTM model, respectively. As we can see from the figures, the LSTM-based dynamic model tends to have considerably higher prediction accuracy over the linear dynamic model. The simplicity of the linear dynamic model is beneficial when identifying parameters in the model (less number of regressor); however, limited flexibility of the model tends to result in a high prediction error, especially in the region where strong non-linear effect occurs. For example, in Fig. 14, linear speed model tends to under-estimate its surge velocity in between 13 s ~ 24 s, however, after 24 s, it over-estimate the surge velocity. This tendency is occurred due to the model's limited flexibility to depict non-linear

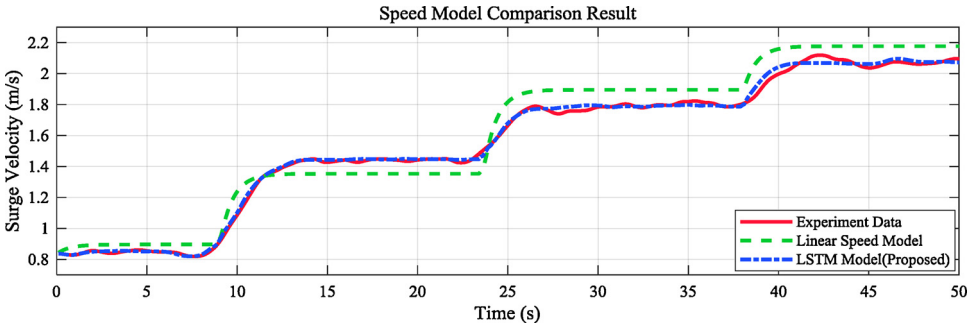

Fig. 14. Observed and predicted surge velocity during an acceleration- deceleration test.

effects in speed dynamics. On the other hand, the complex structure of the LSTM model enables it to have flexibility and high precision for predicting USV dynamics.

Figs. 16 and 17 shows the root mean square (RMS) state prediction error with respect to each dynamical model. State estimation errors are calculated from both training and validation data sets. By comparing the estimation error of validation and training data set, we can analyze the LSTM model's dynamics prediction ability about familiar data and unseen data. Since the LSTM model was trained by the training data set, the model should be able to predict the circumstance corresponds to the data set. Thus, we can assume that if the prediction error of the validation set is similar level as that of the training data set, we may say that model possesses enough capability to describe USV dynamics. Under this assumption, prediction errors of surge velocity, sway velocity and yaw rate are analyzed.

According to the result, surge velocity and yaw rate error prediction error for validation and training sets present similar levels. Which indicates that the trained model can predict dynamics in unseen circumstance with relatively high accuracy. On the other hand, sway velocity prediction error for the validation set tends to have higher values when compared to error estimation of the training set (for the case of Nomoto's with sideslip model, the error in the validation set is 29% higher than that of the training set). This indicates that the sway velocity model still has margin for improvement. Empirically, the estimation of sway velocity tends to be much more complex than the prediction of surge velocity and yaw rate. One reason for this tendency is that the dynamic characteristics of sway velocity is not sufficiently

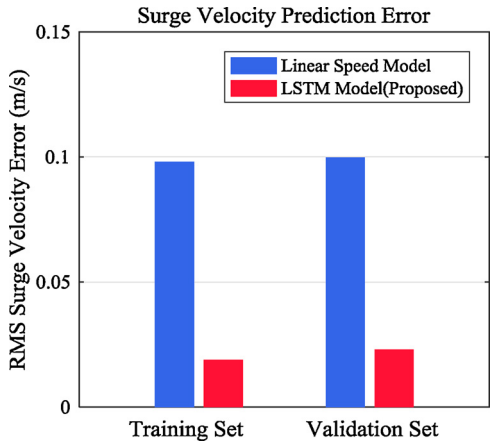

Fig. 16. Performance comparison of the LSTM model and simplified speed models.

distinctive as that of yaw motion. As mentioned in Section 2, our USV platform is a differential thruster type, which means thrusters cannot generate direct sway force. Thus, unlikely in rudder or gimbaled thrusters, the differential thruster is not able to generate sway motion by itself, although small amount of sway velocity motion is made during the turning maneuver. Besides, the sway velocity signal is affected by the sensor noise of both heading angle (GPS compass) and position (GPS) measurement. This uncertainty in sway velocity signal

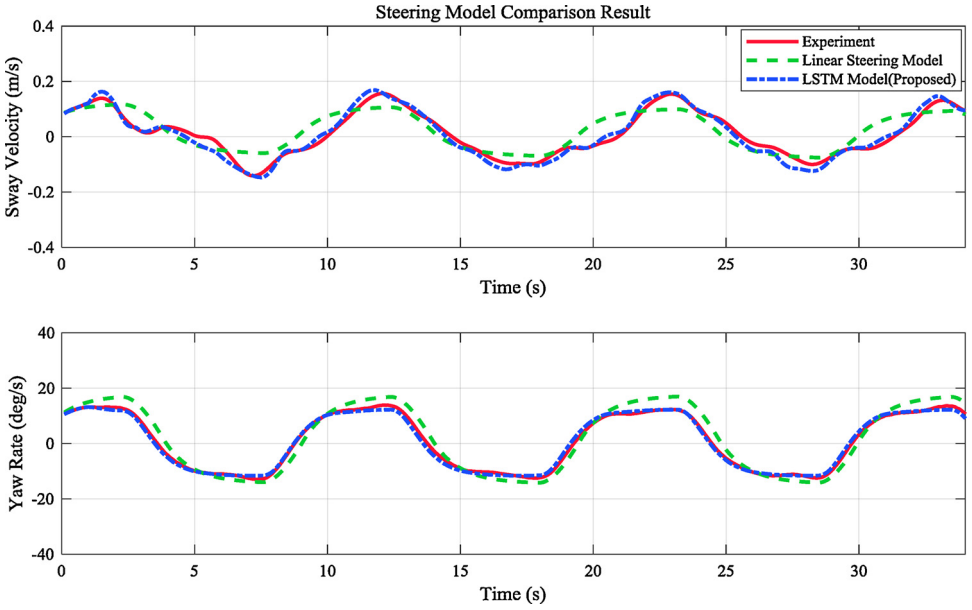

Fig. 15. Observed and predicted sway velocity and yaw rate during a zigzag test.

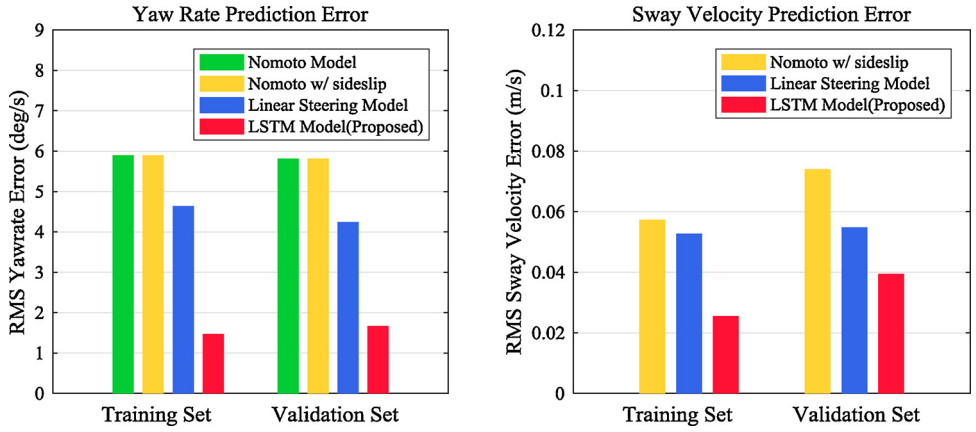

Fig. 17. Performance comparison of the LSTM model and simplified steering models.

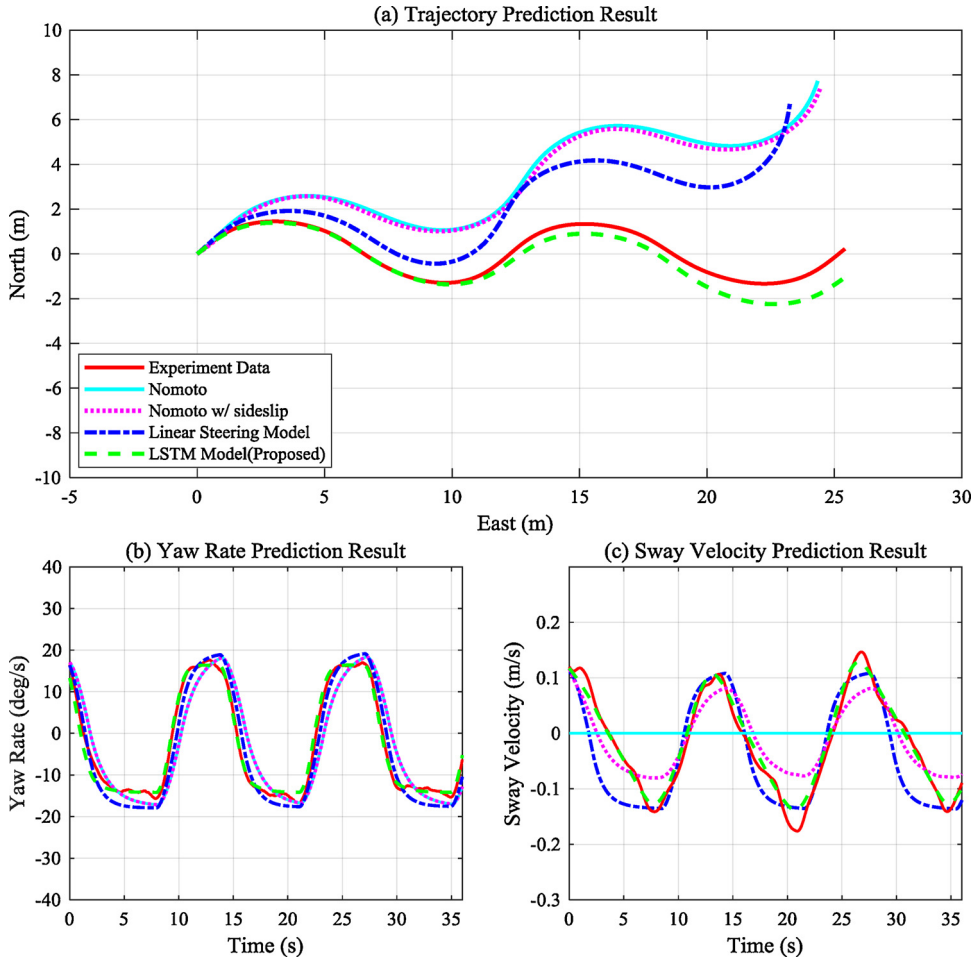

Fig. 18. Observed and predicted trajectory, sway velocity and yaw rate during a zigzag test.

makes it even more difficult to estimate.

In all models (surge, sway and yaw models), LSTM model results significantly outperforms simplified maneuvering models results. The proposed model decreased the surge speed error by 76.9%, the yaw rate error by 60.7% and the sway velocity error by 27.9% compared to the linear dynamic model. Although dynamics prediction ability of the suggested method outperforms that of simplified maneuvering models, it does not guarantee theoretical optimality of the network topologies. One of the reasons for this is the complex structure of the deep neural network (training becomes nonconvex optimization problem). Such complexity of the network often leads to overfitting, interfering it to converge to optimal condition. To prevent this, we adopted anti-overfitting technique such as regularization, or dropout [39] to decrease the level of overfitting.

The increase in dynamics prediction performance can be also observed in Fig.18. Fig.18 shows experiment and simulation results of a zigzag test (10°/0.5). By applying the same control input history of the experimental data to the identified dynamic model, a zigzag test simulation result is calculated. Fig.18(a) shows the trajectory of the experiment and the simulation results, while Figs.18(b) and (c) show the yaw rate and sway velocity history during experiments and simulations, respectively.

In Fig.18, the red solid line represents the experiment data during the test, while the other lines show the prediction result of each model. According to Figs.18(b) and (c), the state prediction performance of LSTM surpasses that of other models. The errors in states (sway velocity, yaw rate) prediction tend to accumulate over the time and eventually will result in positional and angular errors as well. This tendency can be found in Fig.18(a). Because of the accumulation of the state (sway velocity, yaw rate) error, the trajectory error tends to gradually increase. Similarly, the LSTM-based model has the least trajectory error as well.

5. Conclusion

In this work, we suggested a systematic procedure for dynamic system identification of a USV. Based on free running test data, a simplified linear maneuvering model is identified. Although the model can mimic USV dynamics, it is not fully capable of describing complex and coupled non-linear effects in USV dynamics. To overcome this issue, a deep learning–based LSTM architecture for non-linear dynamics prediction was suggested. The LSTM-based dynamic model extracts patterns of USV dynamics from free running test data. The proposed model significantly outperforms conventional simplified maneuvering models. The effectiveness of the proposed method is validated by comparing simulation results and free running test data.

For future work, the constructed dynamical model will be adopted to solve problems such as controller validation or reinforcement learning. In such problems, the use of an accurate dynamic model is critical.

Acknowledgements

This work was supported by (a) Research Institute of Marine Systems Engineering of Seoul National University, (b) Agency for Defense Development (UD160009DD) of Republic of Korea.

References

[1] W. Naeem, et al., UKACC International Control Conference, Modelling and Control of an Unmanned Surface Vehicle for Environmental Monitoring (2006) 1–6.
[2] J. Majohr, T. Buch, Modelling, simulation and control of an autonomous surface marine vehicle for surveying applications Measuring Dolphin MESSIN, IEE Control Engineering Ser. 69 (2006) 329.
[3] O. Levander, Autonomous ships on the high seas, IEEE Spectr. 54 (2) (2017) 26–31.
[4] V. Bertram, Unmanned surface vehicles-a survey, Skibsteknisk Selskab. 1 (2008) 1–14.
[5] R.R. Burgess, Overt persistence: DARPA to sponsor demonstration of USV (unmanned surface vehicle) to shadow submarines, Sea Power 53 (7) (2010) 18–19.
[6] A. Maguer, et al., Turkish International Conference on Acoustics, flashFlash and/or Flash-S Dipping Sonars on Spartan Unmanned Surface Vehicle (USV): A New Asset for Littoral Waters (2005).
[7] W.B. Klinger, et al., Control of an unmanned surface vehicle with uncertain displacement and drag, IEEE J. Ocean. Eng. 42 (2) (2017) 458–476.
[8] H. Ashrafiuon, et al., Sliding-mode tracking control of surface vessels, IEEE Trans. Ind. Electron. 55 (11) (2008) 4004–4012.
[9] M. Caccia, et al., Basic navigation, guidance and control of an unmanned surface vehicle, Auton. Rob. 25 (4) (2008) 349–365.
[10] J. Ghommam, et al., Asymptotic backstepping stabilization of an underactuated surface vessel, IEEE Trans. Control Syst. Technol. 14 (6) (2006) 1150–1157.
[11] Y. Liao, et al., 2010 2nd International Asia Conference on. 1, Combined Speed and Yaw Control of Underactuated Unmanned Surface Vehicles. Informatics in Control, Automation and Robotics (CAR) (2010).
[12] C.R. Sonnenburg, C.A. Woolsey, Modeling, identification, and control of an unmanned surface vehicle, J. Field Rob. 30 (3) (2013) 371–398.
[13] J. Shin, D.J. Kwak, Y.-i. Lee, Adaptive path following control for an unmanned surface vessel using an identified dynamic model, IEEE/ASME Trans. Mechatron. (2017).
[14] W.B. Klinger, et al., Control of an unmanned surface vehicle with uncertain displacement and drag, IEEE J. Ocean Eng. 42 (2) (2017) 458–476.
[15] K.J. Åström, C.G. Källström, Identification of ship steering dynamics, Automatica 12 (1) (1976) 9–22.
[16] H.K. Yoon, K.P. Rhee, Identification of hydrodynamic coefficients in ship maneuvering equations of motion by estimation-before-modeling technique, Ocean Eng. 30 (18) (2003) 2379–2404.
[17] T.I. Fossen, S.I. Sagatun, A.J. Sørensen, Identification of dynamically positioned ships, Control Eng. Pract. 4 (3) (1996) 369–376.
[18] H.D. Nguyen, Recursive identification of ship manoeuvring dynamics and hydrodynamics, ANZIAM J. 49 (2008) 717–732.
[19] R.P. Selvam, S. Bhattacharyya, M. Haddara, A frequency domain system identification method for linear ship maneuvering, Int. Shipbuild. Prog. 52 (1) (2005) 5–27.
[20] G. Rajesh, S. Bhattacharyya, System identification for nonlinear maneuvering of large tankers using artificial neural network, Appl. Ocean Res. 30 (4) (2008) 256–263.
[21] A. Ghosh, S. Raisinghani, S. Khubchandani, Estimation of aircraft lateral-directional parameters using neural networks, J. Aircr. 35 (6) (1998).
[22] A. Punjani, P. Abbeel, Deep learning helicopter dynamics models, IEEE International Conference on. (2015) IEEE, Robotics and Automation (ICRA) (2015).
[23] P. Martin, et al., Neural networks for system identification of coupled ship dynamics, IFAC Proceedings 34 (7) (2001) 83–88.
[24] W. Luo, Z. Zhicheng, Modeling of ship maneuvering motion using neural networks, J. Mar. Sci. Appl. 15 (4) (2016) 426–432.
[25] J. Velagic, Design of ship controller and ship model based on neural network identification structures, Automation Congress WAC 06 World, (2006).
[26] M.R. Dhanak, et al., ASME Offshore Mechanics and Arctic Engineering Conference, Seakeeping Characteristics of a Wave-Adaptive Modular Unmanned Surface Vehicle (2013).
[27] J. Fratello, M. Ahmadian, 11th International Conference on Fast Sea Transportation FAST 2011, Multi-Body Dynamic Simulation and Analysis of Wave-Adaptive Modular Vessels (2011).
[28] T.I. Fossen, Guidance and Control of Ocean Vehicles, John Wiley & Sons Inc, 1994.
[29] T.I. Fossen, Marine Control Systems: Guidance, Navigation and Control of Ships, Rigs and Underwater Vehicles, Marine Cybernetics, 2002.
[30] K. Nomoto, On the steering qualities of ships, Int. Shipbuild. Prog. 4 (35) (1957).
[31] Z. Yu, X. Bao, K. Nonami, Course keeping control of an autonomous boat using low cost sensors, J. Syst. Des. Dyn. 2 (1) (2008) 389–400.
[32] Y. Wang, A new concept using LSTM neural networks for dynamic system identification, IEEE American Control Conference (ACC), 2017 (2017).
[33] S. Hochreiter, J. Schmidhuber, Long short-term memory, Neural Comput. 9 (8) (1997) 1735–1780.
[34] B. Kim, et al., Probabilistic Vehicle Trajectory Prediction Over Occupancy Grid Map via Recurrent Neural Network, arXiv preprint arXiv:1704.07049 (2017).
[35] O. Ogunmolu, et al., Nonlinear Systems Identification Using Deep Dynamic Neural Networks, arXiv preprint arXiv:1610.01439 (2016).
[36] D. Kingma, J. Ba, Adam: A Method for Stochastic Optimization, arXiv preprint arXiv:1412.6980 (2014).
[37] M. Marchand, R. Koehler, Determination of Aircraft Derivatives by Automatic Parameter Adjustment and Frequency Response Methods, AGARD Methods for Aircraft State and Parameter Identification, (1975), p. 18.
[38] A. Savitzky, M.J. Golay, Smoothing and differentiation of data by simplified least squares procedures, Anal. Chem. 36 (8) (1964) 1627–1639.
[39] G. Hinton, et al., Improving Neural Networks by Preventing Co-Adaptation of Feature Detectors, arXiv preprint arXiv:1207.0580 (2012).